Biosensors and Bioelectronics 140 (2019) 111346

Contents lists available at ScienceDirect

Biosensors and Bioelectronics

journal homepage: www.elsevier.com/locate/bios

Multifunctional motion-to-color janus transducers for the rapid detection of sepsis biomarkers in whole blood

Steven M. Russell[a,b], Alejandra Alba-Patiño[a,b], Marcio Borges[a], Roberto de la Rica[a,b,*]

[a] Multidisciplinary Sepsis Group, Balearic Islands Health Research Institute (IdISBa), Son Espases University Hospital, S Building, Carretera de Valldemossa 79, 07120, Palma de Mallorca, Spain

[b] Department of Chemistry, University of the Balearic Islands, Carretera de Valldemossa km 7.5, 07021, Palma de Mallorca, Spain

ARTICLE INFO

Keywords:
Magnetic
Self-propelled
Biosensor
Smartphone
Colorimetric
Procalcitonin

ABSTRACT

Self-propelled particles are revolutionizing sensing applications thanks to a unique motion-based signal generation mechanism in which biorecognition reactions are detected as changes in the velocity of the colloids. Here a new family of self-propelled multifunctional Janus particles is introduced that enables detecting changes in particle motion colorimetrically. The particles consist of an iron oxide core that provides color and magnetism, and a Janus coating that provides biospecific recognition and locomotive properties. In this approach, biomolecular interactions trigger changes in particle motion that are detected as variations in color when spotted on a piece of paper. These variations in color are then read and quantified with a custom-made smartphone app. The high surface area and magnetism of the particles makes them ideal building blocks for developing biosensors because they allow for the rapid capture of a target molecule and the removal of non-specific interactions. Biosensors engineered with the proposed multifunctional particles were able to detect the sepsis biomarker procalcitonin at clinically relevant concentrations within 13 min in whole blood, which is faster than other approaches requiring hour-long incubation steps under controlled conditions to detect the same biomarker in purified serum. The short assay time along with the point-of-need design makes these biosensors suitable for stratifying patients according to their sepsis risk level during triage independently of resource constraints.

1. Introduction

Multifunctional particles are versatile building blocks of hybrid materials that have novel biotechnological applications. For example, multifunctional particles have the potential to simultaneously diagnose and treat diseases, and to imbue biosensors with additional properties to improve their analytical performance (Agusil et al., 2017; Koren et al., 2010; F. Li et al., 2018; Lu et al., 2015; Periyasami et al., 2017; Rosal et al., 2018). The various functions of these particles are made possible by the use of materials with specific physicochemical properties, or by the incorporation of biomolecules, which can endow them with biomolecular recognition and catalytic functions (Pourrahimi and Pumera, 2018). New functions also arise according to the spatial organization of the components in the particles. It is well established that Janus particles with an asymmetric coating of catalysts have locomotive properties mainly due to a bubble thrust (Jurado-Sánchez et al., 2017; Wang et al., 2016; Wu et al., 2015), or a diffusio- or electrophoretic mechanism (Ma et al., 2015; Pourrahimi and Pumera, 2018; Schattling et al., 2015). Multifunctional self-propelled particles have been shown to perform complex tasks autonomously, as evidenced by magnetic self-propelled particles with chemical handles reported to capture and transport cells (Villa et al., 2018). In sensing, it has been demonstrated that self-propulsion can expedite biorecognition reactions (Yu et al., 2014). Moreover, the motion of self-propelled biosensors offers a new way to detect biorecognition reactions when the ligand-receptor interactions change the velocity of the particles. Such changes can be transduced into quantifiable signals by imaging the individual trajectories of a collection of particles and measuring their average velocity. This approach has been successful for the detection of a wide range of targets including pollutants (Orozco et al., 2013; Rojas et al., 2016), disease biomarkers (Yu et al., 2014), viruses (Draz et al., 2018b), oligonucleotides (Van Nguyen and Minteer, 2015) and variations in pH (Su et al., 2016). Recently it has been demonstrated that the trajectories of self-propelled microparticles in a microfluidic chip can be imaged with the camera of a mobile device, therefore paving the way to implement this approach in decentralized analyses performed at

* Corresponding author. Multidisciplinary sepsis group, Balearic Islands Health Research Institute (IdISBa), Son Espases University Hospital, S Building, Carretera de Valldemossa 79, 07120, Palma de Mallorca, Spain.
E-mail address: roberto.delarica@ssib.es (R. de la Rica).

https://doi.org/10.1016/j.bios.2019.111346
Received 19 March 2019; Received in revised form 8 May 2019; Accepted 21 May 2019
Available online 25 May 2019
0956-5663/

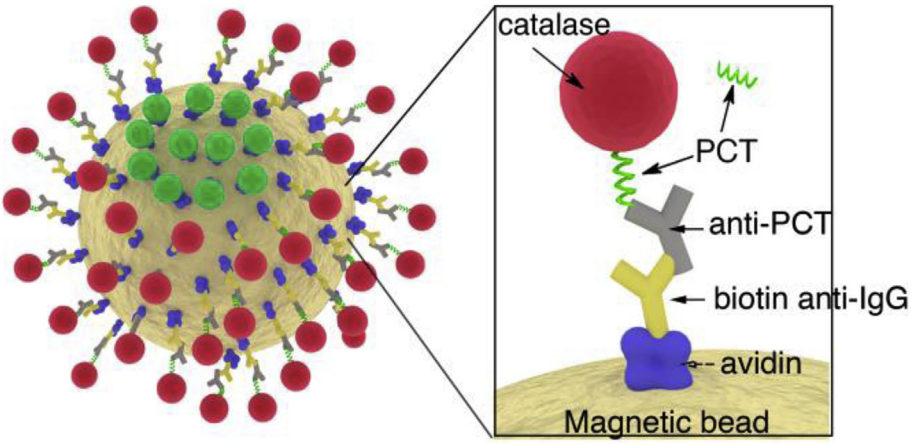

Fig. 1. Schematic representation of the multifunctional Janus particles; The iron oxide core provides magnetic and colorimetric properties, whereas the Janus coating contains anti-PCT antibodies that endow the particles with biorecognition functions. An immunoassay renders the particles covered with catalase, which triggers colloid motion in the presence of H_2O_2.

the point of need (Draz et al., 2018b, 2018a). Expanding this approach for use with nanoparticles, however, faces limitations in terms of imaging and measuring individual trajectories of nanometric objects with only a mobile phone. Another limitation is that the presence of bubbles or dust particles in the microfluidic device may result in spurious results. Finally, mobile phone attachments and microfluidic chips, although inexpensive, are additional pieces of hardware that require transportation and training for use, which impacts their suitability in decentralized settings.

Here we introduce a new family of multifunctional particles that have been designed not only to excel in biosensing, but also to exploit a novel motion-to-color signal generation mechanism for in-field analyses. The particle design is shown in Fig. 1. The particles have a magnetic iron oxide core that enables fast and efficient washing steps in order to remove non-specific interactions in biosensing applications. The characteristic brown color of this material also makes the particles amenable for colorimetry, and the colloidal nature of the biosensor ensures a high surface area for expediting the capture of a target molecule. The iron oxide core is coated with antibodies through avidin-biotin interactions following a Janus design. The antibodies in the Janus coating capture the target molecule by means of a competitive immunoassay (Fig. 2A). This results in the binding of the enzyme catalase to the particles, which generates O_2 bubbles and induces their motion (Keller et al., 2018). Since particle velocity is directly related to the number of enzymes bound to the colloids through biospecific interactions, this approach enables quantifying the concentration of the target molecule by measuring the average velocity of the particles. In our design, the combination of color and self-propulsion in the same particle gives rise to a new method for evaluating changes in the velocity of the particles with densitometry or by visual inspection. To achieve this, the particles are pipetted onto a piece of filter paper, which generates a colored spot (Fig. 2B, left). Upon addition of the enzyme substrate, the particles that captured catalase through antibody-antigen interactions propel themselves. This process yields larger, less colored spots within seconds (Fig. 2B, right). The resulting variations in color are quantified and displayed in real time through an augmented reality interface that uses computer vision algorithms to calculate the relative pixel intensity of the colored spots when viewed through the camera of a smartphone. With this approach, the collective motion of particles can be detected without the need for measuring individual particles, thus eschewing the need for microscopes or special attachments to a mobile phone.

The suitability of the proposed multifunctional particles for developing biosensors was tested for the detection of a sepsis biomarker in whole blood. Sepsis, defined as a multiorgan dysfunction triggered by a dysregulated host response to infection, affects 30 million people and results in the death of around 6 million patients every year. Such high mortality rates could be reduced if sepsis could be quickly diagnosed at an early stage before multi-organ dysfunction becomes irreversible. Procalcitonin (PCT) is one of the most trustworthy biomarkers for rapidly identifying sepsis. This protein is found at undetectable levels ($< 0.05\ ng{\cdot}mL^{-1}$) in the serum of healthy individuals, but its concentration steadily increases to values higher than $2\ ng{\cdot}mL^{-1}$ during sepsis (Meynaar et al., 2011). Although current laboratory tests can detect PCT in about 30 min, PCT tests are generally not performed until a patient arrives to the intensive care unit (ICU), which delays diagnosis and results in a poorer prognosis. A rapid test that could detect PCT in a drop of blood within 10-15 min could help prioritize patients during triage so that they receive life-saving treatments as soon as possible (Reddy et al., 2018). The multifunctional particles reported here are especially engineered to meet this challenge. With our design, the capture of PCT is accelerated by increasing the concentration of particles in contact with the sample, while potential non-specific interactions present in the blood matrix are rapidly removed through magnetic washings. The motion-to-color transduction mechanism generates signals within seconds that are read in real time. The whole assay takes place in a record time of 13 min, therefore making it useful for detecting PCT rapidly at the point of need. Recently biosensors have been proposed for detecting PCT with very low limits of detection. However, they require hour-long incubation steps under controlled temperature conditions (37°C), and therefore they are not suitable for the rapid diagnosis of sepsis. Furthermore, they were only tested in serum, which requires an additional purification step from blood that delays the detection of PCT even more (Chen et al., 2018; C. Li et al., 2018; Sui et al., 2018). Finally, it should be noted that the proposed multifunctional particles could be easily adapted for detecting other blood biomarkers that require rapid detection simply by changing the antibodies in the Janus coating, therefore making them versatile materials for the fabrication of mobile biosensors in decentralized healthcare schemes.

2. Materials and methods

2.1. Fabrication of janus particles

Magnetic beads with a diameter of 1 μm (Dynabeads® MyOne™ Carboxylic Acid, Thermo Scientific) were modified with avidin (Sigma) with the following procedure. First the carboxylic acid groups in 200 μL of beads with a concentration of ca. 10^{10} particles mL^{-1} were transformed into sulfo-NHS esters by adding 2 mg of EDC (N-(3-dimethylaminopropyl)-N′-ethylcarbodiimide hydrochloride, Sigma) and 2 mg of sulfo-NHS (N-hydroxysulfosuccinimide sodium salt, Sigma) dissolved in 500 μL of 0.5 M MES (4-morpholineethanesulfonic acid) pH 5.5. After 20 min the solution was removed with the aid of a magnet and avidin (1 mg dissolved in 0.5 mL of 0.1 M phosphate buffer pH 7.4, Sigma) was added for 1 h. Then 0.5 mL of PBS-BSA ($5\ mg{\cdot}mL^{-1}$ bovine serum albumin in phosphate buffered saline (PBS)) supplemented with 0.1 M

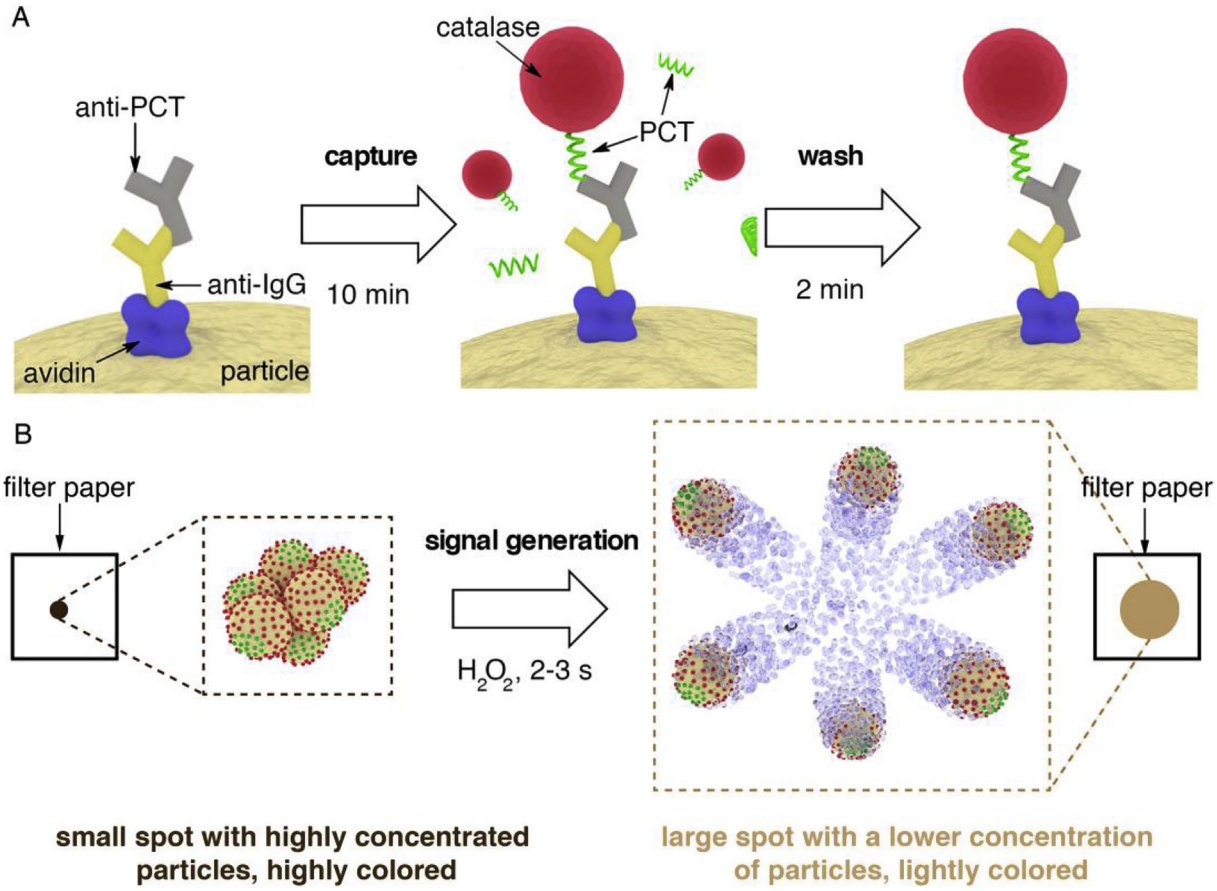

Fig. 2. Schematic representation of the procedure for the rapid detection of PCT with the proposed multifunctional Janus particles; (A) PCT is specifically captured in blood by means of a competitive immunoassay consisting in a 10 min capture step and a 2 min wash procedure; (B) Signal generation mechanism: after spotting the particles on a piece of filter paper H_2O_2 is added; the catalase enzymes generate bubbles that propel the particles and disperse the color within seconds. The subsequent change in pixel intensity is read in real time with a mobile phone app. (For interpretation of the references to color in this figure legend, the reader is referred to the Web version of this article.)

glycine was added for 30 min to block any unreacted sulfo-NHS esters followed by washing 5 times with PBS and re-suspending in a final volume of 200 µL. The resulting avidin-coated beads were kept at 4°C until needed.

The procedure for obtaining a Janus coating of biotin-catalase is schematically showed in Fig. S1. Biotinylated proteins were obtained with an EZ-Link™ sulfo-NHS-biotinylation kit (Thermo Scientific) and purified with a P-10 desalting column. 10 µL of avidin-beads (1:10 dilution in PBST (PBS supplemented with 0.1% Tween-20, Sigma) were added to a 96-well plate previously coated for 1 h with PBS-BSA. A magnet was placed at the bottom of the plate in order to hold the beads in contact with the surface of the well. Then 100 µL of biotin-catalase (10 µg mL^{-1} in PBST) or biotinylated anti-mouse IgG (Fc specific, 10 µg mL^{-1} in PBST Thermo Scientific) was added. After 20 min the solution was carefully removed and the beads were washed with PBST 3 times. Subsequently the magnet was removed and 100 µL of biotinylated BSA (10 µg mL^{-1} in PBST) was added for 30 min to block free biotin-binding sites. The resulting Janus particles were washed 5 times with PBST. Janus particles covered with gold nanoparticles (SEM image in Fig. 3A) were obtained in the same way but substituting biotin-catalase for biotinylated gold nanoparticles. A detailed protocol for the synthesis of the biotinylated gold nanoparticles can be found in the Supplementary Material.

2.2. Characterization of the motion of janus particles

SEM images of the Janus coating were obtained with a Hitachi S-3400N microscope. Particle motion was visualized with an Olympus BX60 microscope. Videos were assembled with ImageJ from images captured every 0.3 s. Particles trajectories and velocities were obtained with MTrackJ. The diffusion coefficient in Fig. 3D was calculated from the size of the particles obtained from dynamic light scattering measurements performed with a Nano Zetasizer instrument (Malvern) using the Stokes equation as previously described (Rucinskaite et al., 2017).

2.3. Motion-to-color signal generation mechanism

To trigger the motion of Janus particles in paper substrates, 0.5 µL of $2{\cdot}10^{10}$ beads mL^{-1} particle suspensions was spotted on a piece of filter paper previously modified with PBS-BSA for 5 min. Then 50 µL of H_2O_2 at concentrations stated in the main text was added. The resulting changes in particle concentration were evaluated with a flatbed scanner and densitometry as stated above. In all experiments, ΔPI represents the increase in pixel density with respect to a blank experiment.

2.4. Detection of procalcitonin

Recombinant human PCT and mouse monoclonal anti-PCT (44d9) were purchased from Invitrogen. The procedure to obtain procalcitonin-conjugated catalase and experiments performed in order to optimize the dilution factor for the competitive immunoassay can be found in the Supplementary Material online. Particles with a Janus coating comprising biotinylated anti-mouse IgG were incubated with mouse anti-PCT (50 µg mL^{-1} in PBST) for 1 h followed by washing 3

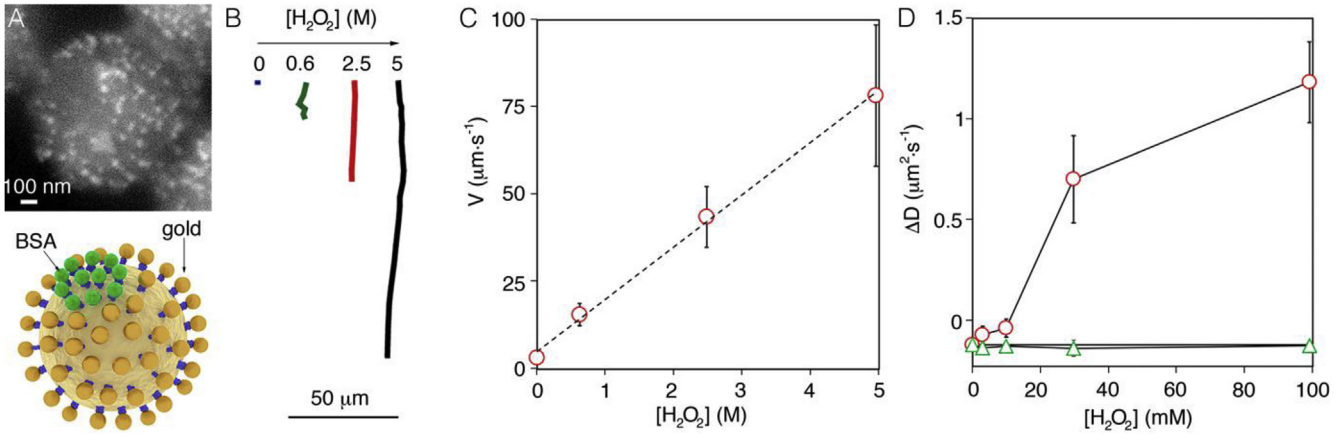

Fig. 3. Characterization of particle motion; (A) SEM image and schematic representation of the Janus coating; (B) Particle trajectories imaged at different concentrations of H_2O_2 for 20 s; (C) Average velocity and standard deviation (error bars) of 10 particles after adding different concentrations of H_2O_2; (D) Increase in diffusion coefficient D of particles modified with active (red dots) or inactive (green triangles) catalase molecules. Error bars are the standard deviation of 3 independent experiments. (For interpretation of the references to color in this figure legend, the reader is referred to the Web version of this article.)

times with PBST. For each experiment, the beads in 10 µL of the resulting particle dispersion were accumulated with a magnet and resuspended in 20 µL of a 1:2 mixture of sample and PCT-conjugated catalase. The sample consisted of recombinant PCT diluted from a 100 µg mL^{-1} stock solution to the desired final concentration using whole blood from healthy volunteers. After 10 min the beads were washed 5 times via a 10 s magnetic accumulation step followed by replacing the solution with 20 µL of fresh PBST. The samples were then resuspended in a final volume of 5 µL and the motion-to-color signal generation mechanism was performed as stated above. Colorimetric signals (S) were obtained in real time with the app that is described in detail in the Supplementary Material.

3. Results and discussion

3.1. Particle motion

The fabrication of the Janus particles is based on a modification of the well-known process of desymmetrization at surfaces that has been described previously (Rucinskaite et al., 2017). A schematic representation of the method can be found in Fig. S1 (Supplementary Material). Briefly, it consists of modifying avidin-decorated particles with biotinylated reagents while holding them on a surface with a magnet. This yields Janus particles with an asymmetric coating of antibodies or enzymes for self-propulsion studies. Then the magnet is removed and free avidin binding sites are blocked with biotinylated BSA. In Fig. 3A, when the procedure was performed with biotinylated gold nanoparticles SEM images showed an asymmetric Janus coating that is in agreement with the design shown in Fig. 1. To test whether a Janus coating containing biotinylated catalase could propel the particles, H_2O_2 was added to a drop of particles and colloid motion was recorded with an optical microscope. In Fig. 3B, analysis of the trajectories of catalase-modified Janus particles upon the addition of H_2O_2 indicates that the particles move longer distances when the concentration of enzyme substrate increases. This agrees well with the idea that biocatalysis is responsible for particle motion. A representative video showing the motion of the particles is also available as Video S1 (Supplementary Material). In this video, all particles move in the same direction, which indicates that they are propelled by convection generated by the collective effervesce. In other instances, particles were filmed moving in a random fashion and being propelled by a deflating O_2 bubble as shown in Fig. S2. These observations suggest that at high H_2O_2 concentrations the particles are mainly propelled by bubbles, either because they are generated on their surface and they thrust the colloids, or because they coalesce and stir the solution where they are suspended. In Fig. 3C the average velocity of 10 particles increases as the concentration of H_2O_2 increases. Oxygen bubbles were visualized in all samples in the concentration range between 0.6 and 5 M. At concentrations below 0.1 M no bubbles were detected, which enabled studying changes in the apparent diffusion coefficient of the particles with dynamic light scattering (DLS) (Ma et al., 2015). In Fig. 3D the diffusion coefficient increases as the concentration of H_2O_2 increases in agreement with the observations in Fig. 3B and C that particle motion depends on the concentration of enzyme substrate. When the same experiments were performed with enzymes that were inactivated by several cycles of freezing and thawing, the diffusion coefficient did not change. This demonstrates that the variations registered in the presence of the active enzymes are originated by their biocatalytic activity. Overall the results shown in Fig. 3 demonstrate that the proposed Janus particles are propelled upon addition of H_2O_2, in agreement with previous reports measuring the velocity and diffusion coefficient of catalase- or nanoplatinum-covered particles (Draz et al., 2018b, 2018a; Ma et al., 2015; Van Nguyen and Minteer, 2015). Below we demonstrate that the motion of the colloids can also be monitored with densitometry when the particles are spotted on a piece of paper, which is the basis for transducing changes in particle motion to colorimetric signals with the mechanism shown in Fig. 2B.

Supplementary video related to this article can be found at https://doi.org/10.1016/j.bios.2019.111346

3.2. Motion-to-color signal generation mechanism

The motion-to-color signal generation mechanism shown in Fig. 2B is based on measuring changes in pixel intensity triggered by the motion of Janus particles spotted on a piece of filter paper. We utilized grade 41 Whatman filter paper with a pore size of 20-25 µm as the substrate. The 3D cellulose mesh can absorb the colloidal suspension and limit particle diffusion in the absence of H_2O_2, while the large pore size allows the particles to disperse upon activation of particle motion. Using paper as the substrate has the additional advantage of enabling quantifying the color of the spot with densitometry, which can be done with a conventional flatbed scanner or through an app installed in a mobile device (Feng et al., 2014; Görücs and Ozcan, 2014; Russell et al., 2017). To demonstrate that the motion of the particles can be detected as a change in the color of a spot, a small drop of highly concentrated catalase-covered Janus particles was first added to a piece of filter paper. Subsequently, a drop of H_2O_2 was added and changes in the pixel intensity of the spot with respect to a blank experiment were measured

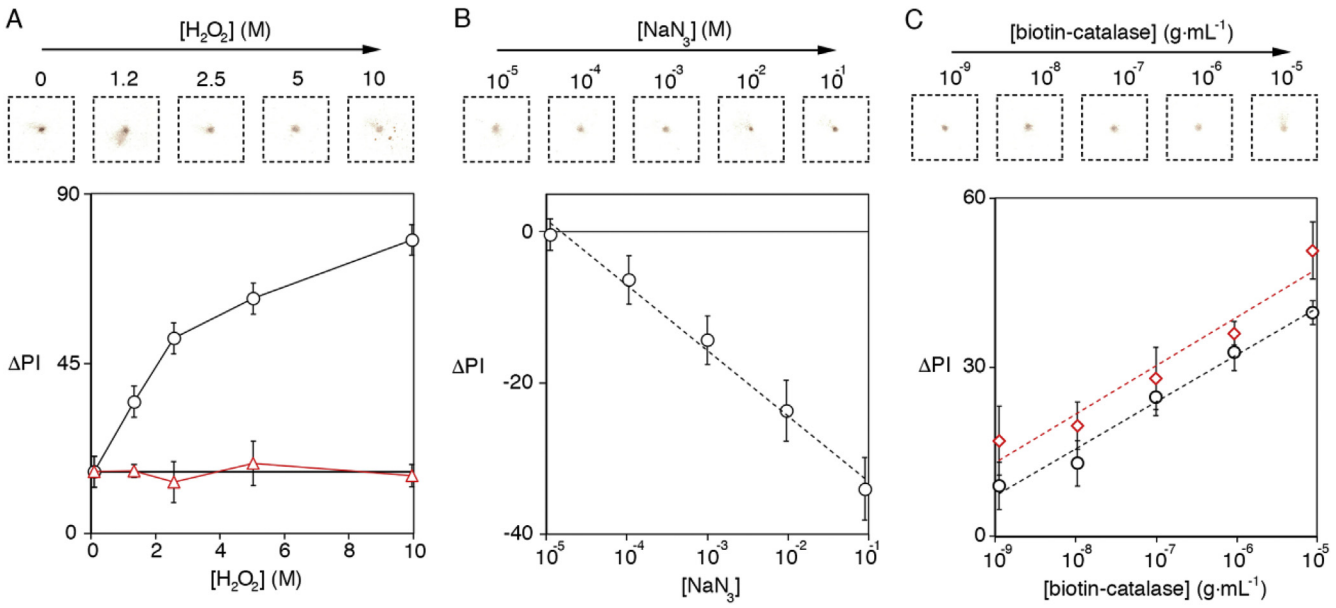

Fig. 4. Motion-to-color signal generation mechanism; Representative scanned images and densitometric analysis of colored spots generated by (A) Janus particles modified with (black dots) or without (red triangles) catalase; (B) Janus particles incubated with the catalase inhibitor sodium azide (semi-logarithmic scale); (C) Janus particles prepared with different concentrations of biotinylated catalase in PBS (black dots, $y = 8.1x + 80$, $r^2 = 0.9$) or incubated for 15 min in whole blood (red diamonds, $y = 8.3x + 88$, $r^2 = 0.9$) (semi-logarithmic scale). Error bars are the standard deviation of 3 independent experiments. (For interpretation of the references to color in this figure legend, the reader is referred to the Web version of this article.)

with a flatbed scanner and quantified with ImageJ. In grayscale, the highest pixel intensity corresponds to white (255), whereas black has a null pixel intensity (0). In Fig. 4A the brown color in the spot fades as the concentration of H_2O_2 increases. At high concentrations of enzyme substrate (5-10 M), bubbles could be seen by eye inspection for 1-3 s on the paper. A closeup view of the process is available as Videos S2 and S3 and Fig. S7 in the Supplementary Materials. In Fig. 4A quantification of the pixel intensity demonstrates that there is a direct relationship between the concentration of H_2O_2 and the colorimetric signal, and control experiments in the absence of catalase indicate that these changes are originated by the enzyme and not by particle etching (red triangles). This demonstrates that the proposed particles can be used to transduce changes in motion into changes in color that, in turn, can be measured with densitometry. To further demonstrate that the colorimetric signal is triggered by the motion of the colloids, the enzymes were inhibited with different concentrations of sodium azide (Beal et al., 2018) and the color in the spot was evaluated after adding a fixed concentration of H_2O_2 (10 M, 50 μL). In Fig. 4B the colorimetric signal decreases as the concentration of inhibitor increases, which further shows that the enzymes are responsible for the change in color.

Supplementary video related to this article can be found at https://doi.org/10.1016/j.bios.2019.111346

We then studied whether the pixel intensity in the spot was affected by the number of catalysts around the particles, which is the basis for applying the motion-to-color mechanism to immunosensing. To this end, Janus particles were prepared by adding different concentrations of biotinylated catalase, and the colorimetric signal generated by the motion of the resulting colloids was studied upon addition of 50 μL of 10 M H_2O_2. In Fig. 4C the variation of pixel intensity with respect to the blank experiment increases linearly as the concentration of biotinylated catalase increases when plotted in a semi-logarithmic scale. This is in agreement with the idea that the motion of the colloids, and therefore the colorimetric signal, is directly related to the number of catalysts in the Janus coating. Finally, we sought to investigate whether the blood matrix could have any effect in the colorimetric signals generated by the catalase-covered Janus particles. This is of particular relevance in the case under study because blood is colored and many blood cells contain catalase, and therefore an inefficient washing step could inadvertently result in the generation of non-specific signals. To rule out this possibility, Janus particles modified with different concentrations of biotinylated catalase were resuspended in whole blood from a healthy donor for 15 min, and then 5 washing steps consisting of 10 s magnetic capturing and liquid substitution with PBST were performed. In Fig. 4C (red diamonds) colorimetric signals are slightly higher but the slope of the linear fitting does not change noticeably when compared to the experiments performed with particles that were not incubated with blood. This shows that the color of the matrix and the presence of catalase in blood does not have a major impact on the sensitivity of the colorimetric sensors, and thus the proposed motion-to-color signal generation mechanism is suitable for blood analyses.

3.3. Detection of procalcitonin (PCT) in blood samples

After demonstrating the motion-to-color signal generation mechanism we sought to implement this concept and the multiple functions of the proposed Janus particles in a biosensor for the detection of PCT in blood. Since every minute counts for diagnosing sepsis at the point of care, we focused on designing a platform capable of detecting concentrations of PCT equal or higher than 2 ng·mL^{-1} in less than 15 min rather than producing a biosensor with higher sensitivity that may require several hours to detect life-threatening levels of PCT. To achieve this goal, the capture of PCT was favored by adding a high concentration of magnetic beads for only 10 min to samples containing the analyte at different levels and PCT conjugated to catalase at a fixed concentration (Figs. S3 and S4). Then 5 washing steps were performed within 2 min to remove non-specific interactions as shown in Fig. 4C. Subsequently the motion-to-color signal generation step was triggered (2-3 s) and the resulting changes in pixel intensity were evaluated in real time with our complementary app (see the Supplementary Material for details about app development). When the assay is viewed through the camera of a mobile device, the app evaluates the image frame every 0.5 s and locates a region of interest (ROI) around the darkest pixel. The ROI contains the darkest pixel and the surrounding area within a 10 pixel diameter of that point in order to calculate the average pixel intensity as an integer value. The integer value is the result of subtracting the average pixel intensity in the ROI from the background value of the

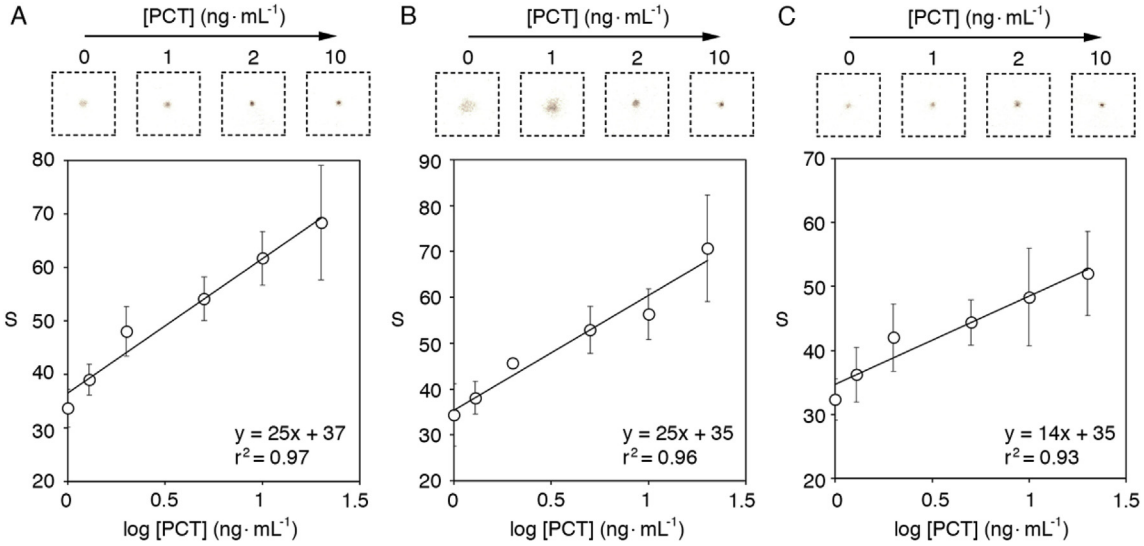

Fig. 5. Detection of PCT in whole blood; Representative scanned images and colorimetric signal (S) generated by PCT spiked into blood from 3 different healthy donors (A, B, C, respectively). Error bars are the standard deviation of 3 independent experiments.

paper substrate. While flatbed scanners control background illumination and eliminate shadows using a built-in light source, our app includes four illumination sensors that alert the user about even or uneven lighting conditions. This allows for the signal to be read in a wide range of ambient lighting conditions and still be free of unwanted light artifacts (Figs. S5 and S6). More specifically, the illumination sensors take the average pixel intensity from four areas on the paper substrate near the ROI and evaluate the evenness of the illumination. When the average pixel intensity for all four illumination sensors are within a narrow range (± 4), the app displays the average pixel intensity of the ROI as a green integer value augmented message over the image in the camera's field of view. If the illumination sensors detect average pixel intensities outside of the established range, it is indicative of uneven illumination and the average pixel intensity of the ROI is displayed in red. Valid measurements are denoted as the colorimetric signal S in the calibration plots for PCT shown in Fig. 5. Please note that background subtraction results in reversed signals compared to results obtained via conventional densitometry in Fig. 4, that is, S is 0 when the color is white and 255 when the color is black. Fig. 5 shows the results for the detection of recombinant PCT spiked into whole blood from 3 different donors. Since healthy volunteers have PCT levels below 0.05 ng·mL^{-1}, its potential contribution to the detection of PCT in the concentration range between 1 and 20 ng·mL^{-1} was deemed negligible. Blood samples from 3 different donors were used in order to account for interpersonal variability in the composition of the matrix. PCT samples at different concentration were obtained by diluting concentrated solutions 1000 times in whole blood. This means that the blood samples were not significantly diluted, and therefore that the spiking procedure did not significantly remove interferences from the matrix. In Fig. 5, the assays yield less colored spots at low concentrations of the target because under this condition the concentration of catalase-PCT bound to the beads is higher, in agreement with the competitive immunoassay format depicted in Fig. 2A. The colorimetric signal S is dose-dependent in the concentration range between 1 and 20 ng·mL^{-1} as shown in the calibration curves depicted in Fig. 5. The blank signal in Fig. 4A, B, and 4C is 24 ± 1, 20 ± 5, and 23 ± 4, respectively. The limit of detection, calculated as the sample that yields a signal higher than 2 times the standard deviation of the blank (95% confidence) is 0.4, 0.6 and 0.7 ng·mL^{-1} for each donor, respectively. The limit of detection calculated as the sample that yields a signal higher than 3 times the standard deviation of the blank (99% confidence) is 0.4, 1 and 1.4 ng·mL^{-1} for each blood matrix, respectively. In all cases, the limit of detection is well below the clinically relevant 2 ng·mL^{-1} threshold value, which demonstrates that the proposed method is useful for detecting alarming levels of PCT rapidly in clinical environments. The detection of the target molecule in a sample as complex as undiluted human blood, which contains a wide array of different proteins and cells at high concentrations, indicates that our method is selective. This is corroborated by detecting PCT with a limit of detection below the 2 ng mL^{-1} threshold value in 3 different matrices from 3 different donors with a 99% level of confidence (Fig. 4A, B, and 4C, respectively). Although the results shown in Fig. 4 are semi-quantitative, the ultrafast turnaround time of our assay makes it useful for prioritizing at-risk patients during triage. Variations of PCT levels in these patients can be subsequently monitored with quantitative laboratory-based methods (Reddy et al., 2018).

4. Conclusions

In conclusion we have introduced multifunctional Janus particles that transduce changes in their motion into changes in color and applied them to the production of colorimetric biosensors. The motion-to-color signal generation mechanism is based on spotting the particles on a piece of paper and measuring changes in pixel intensity triggered by the dispersion of the colloids. Since particle motion depends on the number of enzymes around them, and this parameter in turn depends on the capture of the analyte by the antibodies, the proposed mechanism offers a way to detect target molecules through biospecific interactions in the Janus coating. This signal transduction mechanism is made possible by the combination of color and self-propulsion in the same particle, and has great potential for other colloidal colorimetric probes such as plasmonic nanoparticles that might be difficult to detect with imaging-based approaches. Our particles have other practical attributes, such as a high surface area for the rapid capture of a target molecule with the antibodies in the Janus coating, and magnetic properties for rapid washing steps. Combining all these functions in a single particle allowed us to detect sepsis biomarkers well below the clinically relevant concentration in a record time of 13 min and in whole blood. The proposed biosensors do not require any sample preconditioning steps or bulky instruments, making them suitable for detecting biomarkers at the point of care. Furthermore, the utilization of paper as the sensor substrate makes the proposed signal generation mechanism easy to implement in disposable paper-based analytical devices (Deraney et al., 2016; Russell et al., 2018; Tenda et al., 2018).

Declaration of interests

The authors declare that they have no known competing financial interests or personal relationships that could have appeared to influence the work reported in this paper.

The authors declare the following financial interests/personal relationships which may be considered as potential competing interests:

CRediT authorship contribution statement

Steven M. Russell: Conceptualization, Investigation, Formal analysis, Methodology, Software, Writing - original draft, Writing - review & editing. **Alejandra Alba-Patiño:** Investigation, Formal analysis, Writing - original draft, Writing - review & editing. **Marcio Borges:** Supervision, Writing - original draft, Writing - review & editing. **Roberto de la Rica:** Conceptualization, Data curation, Formal analysis, Funding acquisition, Supervision, Investigation, Methodology, Project administration, Writing - original draft, Writing - review & editing.

Acknowledgement

RR acknowledges financial support from grant CTQ2017-82432-R (MINECO/AEI/FEDER, UE) as well as a Ramón y Cajal contract from Ministerio de Economía, Industria y Competitividad, Agencia Estatal de Investigación, Universitat de les Illes Balears, Conselleria d'Innovació, Recerca i Turisme and the ?European Social Fund. We are grateful to F. Hierro for assistance with SEM imaging.

Appendix A. Supplementary data

Supplementary data to this article can be found online at https://doi.org/10.1016/j.bios.2019.111346.

References

Agusil, J.P., Torras, N., Duch, M., Esteve, J., Pérez-García, L., Samitier, J., Plaza, J.A., 2017. Highly anisotropic suspended planar-array chips with multidimensional submicrometric biomolecular patterns. Adv. Funct. Mater. 27. https://doi.org/10.1002/adfm.201605912.

Beal, N.J., Corry, T.A., O'Malley, P.J., 2018. Comparison of experimental and broken symmetry density functional theory calculated electron paramagnetic resonance parameters for the manganese catalase active site in the superoxidized MnIII/MnIVState. J. Phys. Chem. B 122, 2881–2890. https://doi.org/10.1021/acs.jpcb.7b11649.

Chen, P., Qiao, X., Liu, J., Xia, F., Tian, D., Zhou, C., 2018. A dual-signals response electrochemiluminescence immunosensor based on PTC-DEPA/KCC-1 NCs for detection of procalcitonin. Sensor. Actuator. B Chem. 267, 525–532. https://doi.org/10.1016/j.snb.2018.04.061.

Deraney, R.N., Mace, C.R., Rolland, J.P., Schonhorn, J.E., 2016. Multiplexed, patterned-paper immunoassay for detection of malaria and dengue fever. Anal. Chem. 88, 6161–6165. https://doi.org/10.1021/acs.analchem.6b00854.

Draz, M.S., Kochehbyoki, K.M., Vasan, A., Battalapalli, D., Sreeram, A., Kanakasabapathy, M.K., Kallakuri, S., Tsibris, A., Kuritzkes, D.R., Shafiee, H., 2018a. DNA engineered micromotors powered by metal nanoparticles for motion based cellphone diagnostics. Nat. Commun. 9, 4282. https://doi.org/10.1038/s41467-018-06727-8.

Draz, M.S., Lakshminaraasimulu, N.K., Krishnakumar, S., Battalapalli, D., Vasan, A., Kanakasabapathy, M.K., Sreeram, A., Kallakuri, S., Thirumalaraju, P., Li, Y., Hua, S., Yu, X.G., Kuritzkes, D.R., Shafiee, H., 2018b. Motion-based immunological detection of zika virus using Pt-nanomotors and a cellphone. ACS Nano 12, 5709–5718. https://doi.org/10.1021/acsnano.8b01515.

Feng, S., Caire, R., Cortazar, B., Turan, M., Wong, A., 2014. Immunochromatographic diagnostic test analysis using google glass. ACS Nano 3069–3079. https://doi.org/10.1021/nn500614k.

Göröcs, Z., Ozcan, A., 2014. Biomedical imaging and sensing using flatbed scanners. Lab Chip 14, 3248–3257. https://doi.org/10.1039/c4lc00530a.

Jurado-Sánchez, B., Pacheco, M., Rojo, J., Escarpa, A., 2017. Magnetocatalytic graphene quantum dots Janus micromotors for bacterial endotoxin detection. Angew. Chem. Int. Ed. 56, 6957–6961. https://doi.org/10.1002/anie.201701396.

Keller, S., Teora, S.P., Hu, G.X., Nijemeisland, M., Wilson, D.A., 2018. High-throughput design of biocompatible enzyme-based hydrogel microparticles with autonomous movement. Angew. Chem. Int. Ed. 57, 9814–9817. https://doi.org/10.1002/anie.201805661.

Koren, K., Scheucher, E., Aigner, D., Klimant, I., Borisov, S.M., Zankel, A., Po, P., 2010. Multifunctional magnetic optical sensor particles with tunable sizes for monitoring metabolic parameters and as a basis for nanotherapeutics. Adv. Funct. Mater. 20, 1842–1851. https://doi.org/10.1002/adfm.201000321.

Li, C., Zhang, R., Liu, P., Tang, Q., Shen, P., Wei, J., Lu, Y., 2018. An ultrasensitive electrochemical immunosensor for procalcitonin detection based on the gold nanoparticles-enhanced tyramide signal amplification strategy. Biosens. Bioelectron. 126, 543–550. https://doi.org/10.1016/j.bios.2018.10.048.

Li, F., Wang, C., Guo, W., 2018. Multifunctional poly- N -isopropylacrylamide/DNAzyme microgels as highly efficient and recyclable catalysts for biosensing. Adv. Funct. Mater. 28, 1705876. https://doi.org/10.1002/adfm.201705876.

Lu, C., Liu, X., Li, Y., Yu, F., Tang, L., Hu, Y., Ying, Y., 2015. Multifunctional Janus hematite-silica nanoparticles: mimicking peroxidase-like activity and sensitive colorimetric detection of glucose. ACS Appl. Mater. Interfaces 7, 15395–15402. https://doi.org/10.1021/acsami.5b03423.

Ma, X., Jannasch, A., Albrecht, U.-R., Hahn, K., Miguel-López, A., Schäffer, E., Sánchez, S., 2015. Enzyme-Powered hollow mesoporous Janus nanomotors. Nano Lett. 15, 7043–7050. https://doi.org/10.1021/acs.nanolett.5b03100.

Meynaar, I.A., Droog, W., Batstra, M., Vreede, R., Herbrink, P., 2011. In Critically ill patients, serum procalcitonin is more useful in differentiating between sepsis and SIRS than CRP, il-6, or LBP. Crit. Care Res. Pract. 2011, 594645. https://doi.org/10.1155/2011/594645.

Orozco, J., García-Gradilla, V., D'Agostino, M., Gao, W., Cortés, A., Wang, J., 2013. Artificial enzyme-powered microfish for water-quality testing. ACS Nano 7, 818–824. https://doi.org/10.1021/nn305372n.

Periyasami, G., Alrohaili, A., Shi, J., Song, S., 2017. Multifunctional yolk − shell nanostructure as a superquencher for fluorescent analysis of potassium ion using guanine-rich oligonucleotides. ACS Appl. Mater. Interfaces 9, 30406–30413. https://doi.org/10.1021/acsami.7b08732.

Pourrahimi, A.M., Pumera, M., 2018. Multifunctional and self-propelled spherical Janus nano/micromotors: recent advances. Nanoscale 10, 16398–16415. https://doi.org/10.1039/c8nr05196h.

Reddy Jr., B., Hassan, U., Seymour, C., Angus, D.C., Isbell, T.S., White, K., Weir, W., Yeh, L., Vincent, A., Bashir, R., 2018. Point-of-care sensors for the management of sepsis. Nat. Biomed. Eng. 2, 640–648. https://doi.org/10.1038/s41551-018-0288-9.

Rojas, D., Jurado-Sánchez, B., Escarpa, A., 2016. "Shoot and sense" Janus micromotors-based strategy for the simultaneous degradation and detection of persistent organic pollutants in food and biological samples. Anal. Chem. 88, 4153–4160. https://doi.org/10.1021/acs.analchem.6b00574.

Rosal, B., Jia, B., Jaque, D., 2018. Beyond Phototherapy : recent advances in multifunctional fluorescent nanoparticles for light-triggered tumor theranostics. Adv. Funct. Mater. 28, 1803733. https://doi.org/10.1002/adfm.201803733.

Rucinskaite, G., Thompson, S.A., Paterson, S., de la Rica, R., 2017. Enzyme-coated Janus nanoparticles that selectively bind cell receptors as a function of the concentration of glucose. Nanoscale 9, 5404–5407. https://doi.org/10.1039/C7NR00298J.

Russell, S.M., Alba-Patiño, A., Borges, M., de la Rica, R., 2018. A robust and user-friendly alternative to densitometry using origami biosensors and digital logic. ACS Sens. 3, 1712–1718. https://doi.org/10.1021/acssensors.8b00452.

Russell, S.M., Domenech-Sanchez, A., de la Rica, R., 2017. Augmented reality for real-time detection and interpretation of colorimetric signals generated by paper-based biosensors. ACS Sens. 2, 848–853. https://doi.org/10.1021/acssensors.7b00259.

Schattling, P., Thingholm, B., Städler, B., 2015. Enhanced diffusion of glucose-fueled Janus particles. Chem. Mater. 27, 7412–7418. https://doi.org/10.1021/acs.chemmater.5b03303.

Su, Y., Ge, Y., Liu, L., Zhang, L., Liu, M., Sun, Y., Zhang, H., Dong, B., 2016. Motion-based pH sensing based on the cartridge-case-like micromotor. ACS Appl. Mater. Interfaces 8, 4250–4257. https://doi.org/10.1021/acsami.6b00012.

Sui, Y., Xu, A., Jin, X., Zheng, J., He, X., Cheng, Y., Xie, Q., Liu, R., 2018. In situ enzymatic generation of gold for ultrasensitive amperometric sandwich immunoassay of procalcitonin. Biosens. Bioelectron. 117, 422–428. https://doi.org/10.1016/j.bios.2018.06.037.

Tenda, K., van Gerven, B., Arts, R., Hiruta, Y., Merkx, M., Citterio, D., 2018. Paper-based antibody detection devices using bioluminescent BRET-switching sensor proteins. Angew. Chem. Int. Ed. 57, 15369–15373. https://doi.org/10.1002/anie.201808070.

Van Nguyen, K., Minteer, S.D., 2015. DNA-functionalized Pt nanoparticles as catalysts for chemically powered micromotors: toward signal-on motion-based DNA biosensor. Chem. Commun. 51, 4782–4784. https://doi.org/10.1039/C4CC10250A.

Villa, K., Krejčová, L., Novotný, F., Heger, Z., Sofer, Z., Pumera, M., 2018. Cooperative multifunctional self-propelled paramagnetic microrobots with chemical handles for cell manipulation and drug delivery. Adv. Funct. Mater. 28, 1804343. https://doi.org/10.1002/adfm.201804343.

Wang, H., Moo, J.G.S., Pumera, M., 2016. From nanomotors to micromotors: the influence of the size of an autonomous bubble-propelled device upon its motion. ACS Nano 10, 5041–5050. https://doi.org/10.1021/acsnano.5b07771.

Wu, Z., Li, J., de Ávila, B.E.-F., Li, T., Gao, W., He, Q., Zhang, L., Wang, J., 2015. Water-Powered cell-mimicking Janus micromotor. Adv. Funct. Mater. 25, 7497–7501. https://doi.org/10.1002/adfm.201503441.

Yu, X., Li, Y., Wu, J., Ju, H., 2014. Motor-based autonomous microsensor for motion and counting immunoassay of cancer biomarker. Anal. Chem. 86, 4501–4507. https://doi.org/10.1021/ac500912c.